



Article (refereed) – Published version

Moat, B.I.; Josey, S.; Sinha, B.. 2014 Impact of Barents Sea winter air-sea exchanges on Fram Strait dense water transport. *Journal of Geophysical Research*, 119 (2). 1009-1021. [10.1002/2013JC009220](https://doi.org/10.1002/2013JC009220)

This version available at <http://nora.nerc.ac.uk/504573/>

NERC has developed NORA to enable users to access research outputs wholly or partially funded by NERC. Copyright and other rights for material on this site are retained by the rights owners. Users should read the terms and conditions of use of this material at <http://nora.nerc.ac.uk/policies.html#access>

AGU Publisher statement: An edited version of this paper was published by AGU. Copyright (2014) American Geophysical Union. Further reproduction or electronic distribution is not permitted.

Moat, B.I.; Josey, S.; Sinha, B.. 2014 Impact of Barents Sea winter air-sea exchanges on Fram Strait dense water transport. *Journal of Geophysical Research*, 119 (2). 1009-1021. [10.1002/2013JC009220](https://doi.org/10.1002/2013JC009220)

To view the published open abstract, go to <http://dx.doi.org/10.1002/2013JC009220>

Contact NOC NORA team at
publications@noc.soton.ac.uk

RESEARCH ARTICLE

10.1002/2013JC009220

Impact of Barents Sea winter air-sea exchanges on Fram Strait dense water transport

Bengamin I. Moat¹, Simon A. Josey¹, and Bablu Sinha¹¹National Oceanography Centre, University of Southampton Waterfront Campus, European Way, Southampton, UK

Key Points:

- Impacts of extreme Barents Sea surface exchanges examined using climate model
- Barents Sea surface density gain increases Fram Strait southward transport
- Fram Strait dense water colder (fresher) by up to 0.5°C (0.05)

Correspondence to:

B. I. Moat,
ben.moat@noc.ac.uk

Citation:

Moat, B. I., S. A. Josey, and B. Sinha (2014), Impact of Barents Sea winter air-sea exchanges on Fram Strait dense water transport, *J. Geophys. Res. Oceans*, 119, 1009–1021, doi:10.1002/2013JC009220.

Received 18 JUNE 2013

Accepted 17 JAN 2014

Accepted article online 22 JAN 2014

Published online 12 FEB 2014

Abstract Impacts of extreme Barents Sea air-sea exchanges are examined using the HadCM3 coupled ocean-atmosphere model. Variability in the Barents Sea winter air-sea density flux is found to be a potentially significant factor in determining changes in the southward transport of dense water through Fram Strait. The density flux variability is primarily driven by the thermal term, F_T , due to heat loss to the atmosphere. The other two terms (haline flux and ice formation) play a relatively minor role. The difference in ocean circulation between winters with extreme strong and weak Barents Sea surface density flux anomalies is analyzed. This reveals an increase in strong winters of both the north-westward intermediate depth flow out of the basin and the east-west deep flows north of Spitsbergen and south through the Fram Strait. A linear fit yields a Fram Strait southward transport increase of 1.22 Sv for an increase in F_T of $1 \times 10^{-6} \text{ kg m}^{-2} \text{ s}^{-1}$. For the 10 strongest Barents Sea surface density flux winters, the Fram Strait winter southward transport increases by 2.4 Sv. This compares with a reduction of 1.0 Sv for the corresponding weakest winters. Furthermore, the properties of the southward flowing water are modified in strong density flux winters. In such winters, the Fram Strait water below 250 m is colder by up to 0.5°C and fresher by 0.05 than the climatological winter mean.

1. Introduction

Variations in the transports of heat and freshwater through Fram Strait may cause changes in the global ocean circulation through their influence on Greenland Sea and Labrador Sea dense water formation [Vellinga and Wood, 2002; Stouffer *et al.*, 2006; Myers, 2005]. These transports are expected to be influenced by a range of processes including: (i) warming of North Atlantic inflow through the Fram Strait [Schauer *et al.*, 2004; Walczowski and Piechura, 2007; Holliday *et al.*, 2008; Beszczynska-Möller *et al.*, 2012], (ii) changes in the wind stress curl field [Giles *et al.*, 2012], and (iii) variations in the strength of air-sea buoyancy loss and related dense water formation in neighboring seas. The last of these processes has not been considered in detail previously. We explore it here, focusing on the Barents Sea, through analysis of a coupled ocean-atmosphere model.

The Barents Sea is a relatively shallow shelf sea, which has recently experienced the largest sea ice retreat in the Arctic [Cavalieri and Parkinson, 2012, Figure 3g]. As the relatively warm North Atlantic Water (NAW) flows northward toward this region it splits into two main branches (see Figure 1). One branch enters the Barents Sea between Bear Island and Norway, while the other proceeds north through Fram Strait. The NAW entering the Barents Sea becomes colder, less saline, and denser in the south of the region. A component flows out in winter into the Nansen Basin through the St. Anna Trough [Schauer *et al.*, 2002; Rudels *et al.*, 2004; Aksenov *et al.*, 2011]. This modified NAW outflow contributes to formation of between 50% and 80% of the Arctic Intermediate Water (AIW) [Schauer *et al.*, 1997] in the Nansen Basin. The AIW subsequently returns to the North Atlantic through the Fram Strait on a time scale of order 20 years [Newton *et al.*, 2008; Smith *et al.*, 2011]. In addition, there is a small outflow from the Barents Sea through the strait between Spitsbergen and Franz Josef Land [Loeng *et al.*, 1997], referred to subsequently as the SFJL Strait. The Barents Sea ice extent is controlled, in part, by the recent strengthening and warming of the NAW inflow [Árthun *et al.*, 2012].

Within the Barents Sea, the NAW may become colder as a result of intense air-sea heat loss. This intense loss results from exposure to the atmosphere in ice-free open water and in short-lived polynyas. Its salinity is modified through mixing of the cooled NAW with brine rich waters from ice formation, and freshwater from river runoff and precipitation. The heat transport into the Barents Sea modulates both its mean

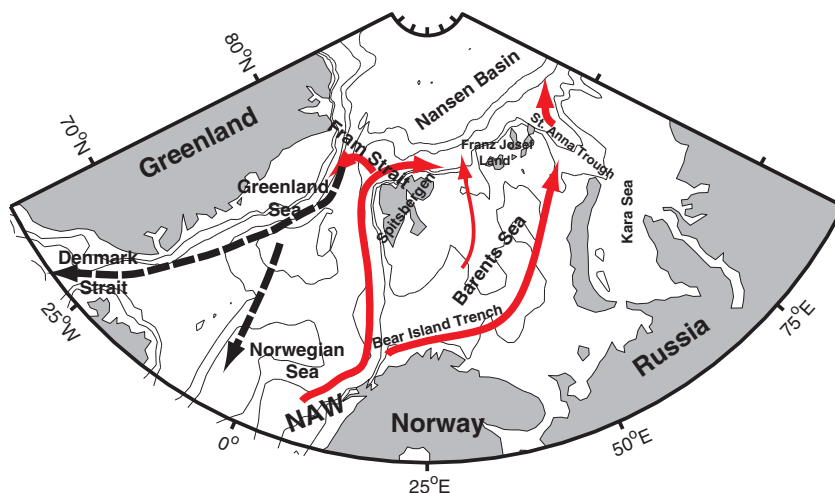


Figure 1. Schematic of the general circulation and bathymetry of the Barents and Greenland Seas. The thick red solid lines indicate the relatively warm North Atlantic Water (NAW) entering the Arctic and Barents Seas. The dashed black lines indicate the dense deep return flow.

temperature and the area over which the cooling occurs [Schauer *et al.*, 2002, Smedsrud *et al.*, 2010]. In particular, when the heat transport is high the warmer water spreads further into the basin enabling cooling over a larger area. However, the detailed relationship between the surface buoyancy flux forcing in the Barents Sea and outflows from the basin has yet to be determined.

In the study reported here, we explore this relationship with a focus on the consequences of enhanced Barents Sea surface heat loss. Our approach is to use a 1000 year long preindustrial control run of the coupled ocean-atmosphere model, HadCM3. The long period spanned by the run enables such a study as it samples a very wide range of air-sea interaction conditions. For example, winter mean net air-sea heat flux ranges from -203 to -46 W m^{-2} on average in strong and weak heat loss years (see section 3.2). Note, heat flux is defined to be negative for ocean heat loss throughout our analysis. Thus, we are able to isolate extreme heat loss events and determine their impacts on the regional ocean circulation. In particular, we examine whether changes in Barents Sea dense water formation have potential consequences for the SFJL Strait outflow and the Fram Strait transport. The magnitude of the outflow is very uncertain given the limited observations available but thought to be small [Loeng *et al.*, 1997].

We stress that we are not trying to use the HadCM3 control run to directly simulate changes in the Barents Sea in recent decades. Recent rapid changes in Barents Sea ice cover open up the possibility for greatly enhanced heat loss in winter and an increase in dense water formation. The enhanced loss is likely to have a spatial dependence on the location of the sea ice edge [Day *et al.*, 2012]. Continuing reductions in ice cover expected in the next few decades [Stroeve *et al.*, 2012; Wang and Overland, 2009] may further enhance this process. Simulation of the impacts of these recent changes requires a model that accurately represents forcing conditions, ocean circulation, and hydrography over the past few decades. Such a simulation is beyond the scope of the present study.

Our research builds on two earlier analyses that used coupled models to determine the influence of Greenland Sea extreme heat loss on the southward transport of dense water through Denmark Strait [Grist *et al.*, 2007, 2008]. In Grist *et al.* [2007], we showed using HadCM3 that deep water transport through Denmark Strait increases by about 30% between strong and weak heat loss events in the Greenland Sea. Subsequently, we explored in detail the propagation time scale and pathway of the surface heat loss driven cold anomalies through the Denmark Strait [Grist *et al.*, 2008]. Here, we employ the techniques used in these earlier studies to investigate the potential response of the Fram Strait transport to extreme winter heat loss in the Barents Sea. The paper is organized as follows. Details of the HadCM3 model and analysis method are given in section 2. The results of our analysis are presented in section 3 and the key issues are drawn together and discussed in section 4.

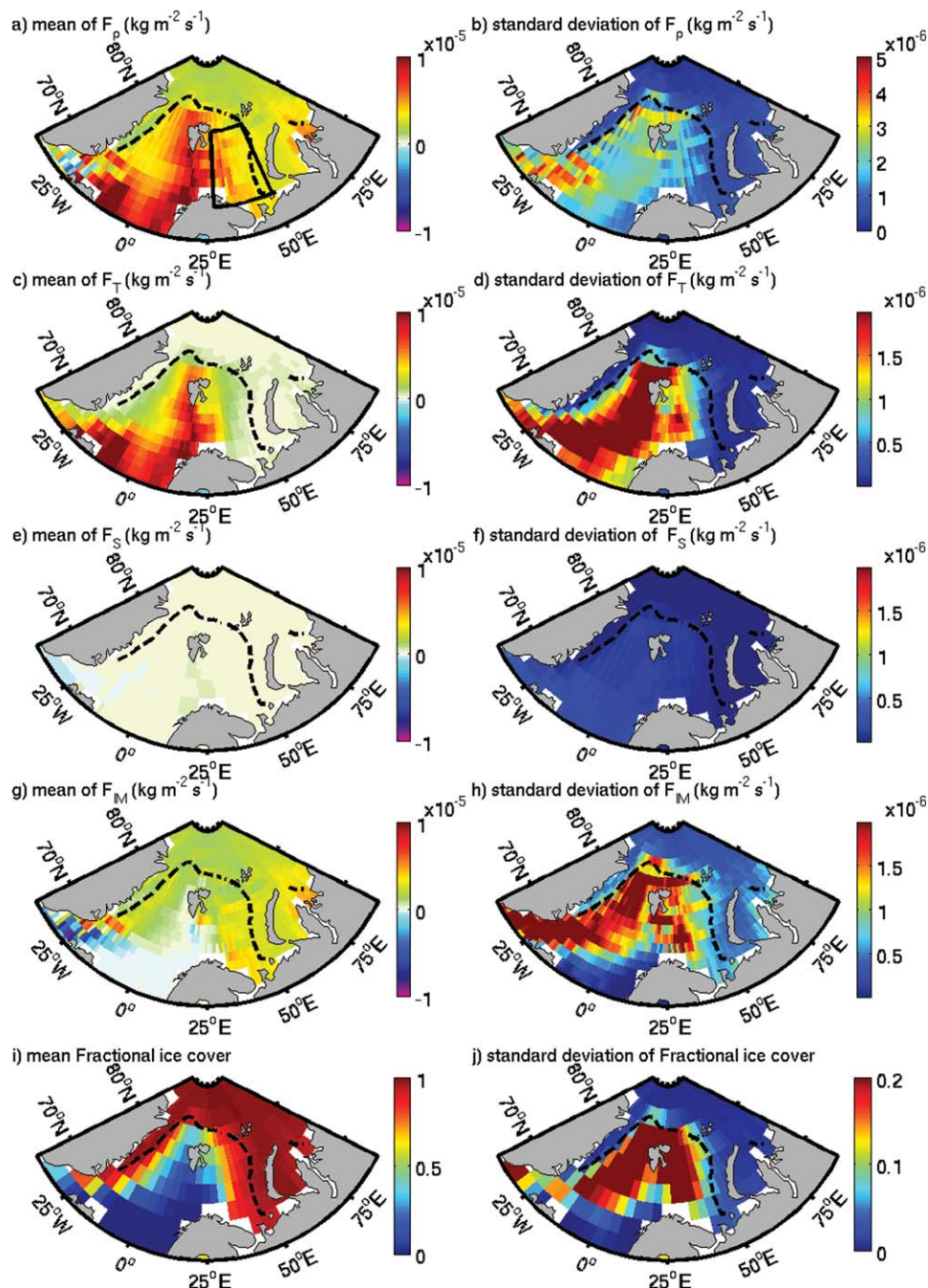


Figure 2. (left) HadCM3 control run winter mean and (right) standard deviation of the mean surface density flux fields (units $\text{kg m}^{-2} \text{s}^{-1}$): (a and b) F_p , (c and d) F_T , (e and f) F_s , (g and h) F_M , and (i and j) mean and standard deviation of the fractional ice cover. The black dashed lines indicate the climatological mean winter sea ice extent at 95% cover. Black solid lines in Figure 2a indicate the Barents Sea box referred to in section 3.2.

2. Model and Method

2.1. Model Characteristics

We have analyzed output from a 1000 year control run of the coupled ocean-atmosphere model HadCM3 with fixed preindustrial greenhouse gases. The main characteristics of the model are briefly summarized here; for full details, see *Gordon et al.* [2000]. HadCM3 has 19 vertical levels in the atmosphere with a horizontal resolution of $2.5^\circ \times 3.75^\circ$ and 20 depth levels in the ocean with a horizontal resolution of $1.25^\circ \times 1.25^\circ$. The model atmospheric time step is 30 min and the atmosphere and ocean components are coupled

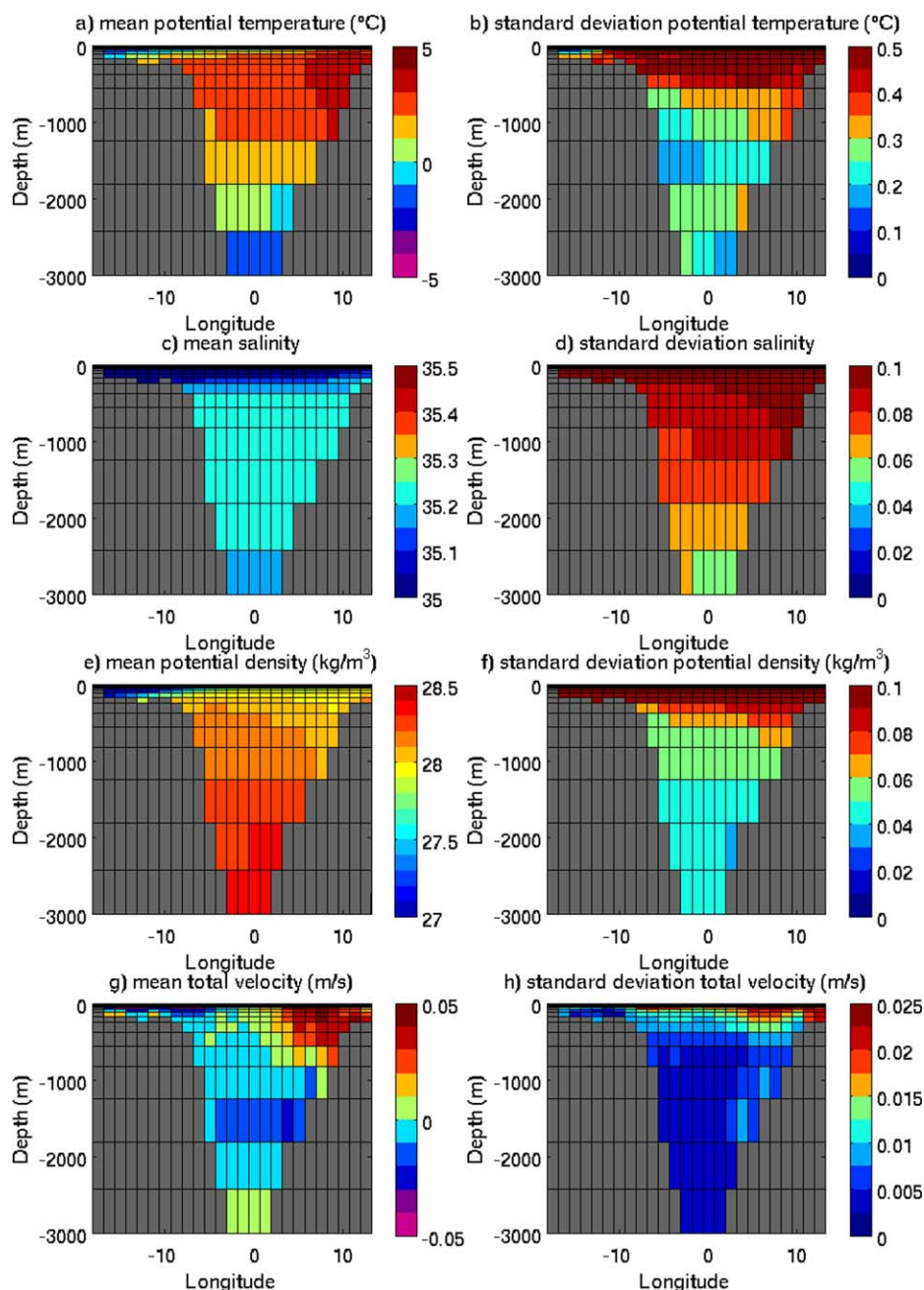


Figure 3. HadCM3 control run winter mean and standard deviation fields for the 78.75°N section through Fram Strait (a and b) temperature; (c and d) salinity; (e and f) potential density; (g and h) velocity. Velocities are positive for northward moving water.

once per day. The model takes about 400 years for the heat and freshwater budgets to become balanced, after which it exhibits a stable climate without the need for flux corrections. We have used output in the interval from model year 1850 to 2849 that is the 1000 year section that falls after the initial 400 years of integration.

Gordon *et al.* [2000] discuss the main characteristics of the control run and many subsequent studies have employed HadCM3 to examine a wide variety of climate system processes. For example, Sinha *et al.* [2013] used the model to study the impacts of westward propagating baroclinic Rossby waves. These are generated by fluctuations in wind stress curl on the eastern boundary and are found to have an important effect on the variability and predictability of North Atlantic meridional transports. Of relevance to the present study, forced experiments with HadCM3 have been able to capture observed recent Arctic climate change.

For example, the decline of sea ice area and volume [Gregory *et al.*, 2002; Ridley *et al.*, 2012] and increases in river discharges into the Arctic Ocean since the 1960s [Wu *et al.*, 2005]. As noted in section 1, we have previously employed it to study heat loss impacts on the Denmark Strait transport [Grist *et al.*, 2007, 2008].

2.2. Analysis Details

As a measure of the combined influence of air-sea heat and freshwater loss, and ice melt, on the surface water density we employ the total surface density flux, F_ρ , given by:

$$F_\rho = F_T + F_S + F_{IM} \quad (1)$$

Here, the different contributions are the thermal component (F_T), and two haline components, the net evaporative density flux (F_S), and the ice melt/formation density flux (F_{IM}). These are defined as follows:

$$F_T = -\alpha \frac{Q_{net}}{C_p} \quad (2)$$

$$F_S = \alpha \beta S \frac{E - P}{(1 - S/1000)} \quad (3)$$

$$F_{IM} = \rho \alpha \beta S \frac{I_M}{(1 - S/1000)} \quad (4)$$

Here ρ is the density of water at the sea surface, C_p is the specific heat capacity of water, S is sea surface salinity (measured on the Practical Salinity Scale), Q_{net} is the net heat flux (defined to be positive for heat gain by the ocean from the atmosphere), $E - P$ is the net evaporation at the ocean surface and I_M is the freshwater flux associated with ice formation or melt (defined to be negative for net freshwater input into the ocean, i.e., as a result of ice melt). Note that Q_{net} is the sum of contributions from four heat flux components: the sensible, latent, longwave, and shortwave fluxes. The terms α and β are the thermal expansion and haline contraction coefficients, respectively,

$$\alpha = -\frac{1}{\rho} \frac{\partial \rho}{\partial T} \quad (5)$$

$$\beta = -\frac{1}{\rho} \frac{\partial \rho}{\partial S} \quad (6)$$

Values for ρ , C_p , α , and β have been calculated using equations summarized by Gill [1982, Appendix 3].

Our analysis focuses on winter (defined to be December–March, DJFM) as this is the season of maximum heat loss. Time series of winter mean Barents Sea air-sea density flux and southward Fram Strait dense water volume transport (using a section along 78.75°N) have been determined from HadCM3. Dense water is defined to be water denser than 27.0 kg m⁻³. This threshold is chosen to separate the light surface southward transport of the East Greenland Current from waters transformed to denser water classes in the region. Each time series has been linearly detrended prior to calculation of correlation statistics.

3. Results

3.1. Winter Mean Surface Density Flux and Fram Strait Transport Properties

The HadCM3 1000 year run winter mean surface density flux in the Barents Sea and adjacent regions, together with its components, is shown in Figure 2. The dashed lines show the model climatological mean winter sea ice extent at 95% cover. Over open water, the thermal term dominates the contribution to the density flux in the mean with much smaller values for F_S . The thermal term tends to increase water density (i.e., there is a positive density flux which corresponds to net heat loss) with high values in the western Barents and Norwegian Seas (F_T up to 10⁻⁵ kg m⁻² s⁻¹). By comparison, F_S is typically two orders of magnitude smaller (order 10⁻⁷ kg m⁻² s⁻¹) over the whole region. The contribution of ice melt/formation, F_{IM} , over most of the region is positive due to brine rejection associated with ice formation, reaching values up

to $7 \times 10^{-6} \text{ kg m}^{-2} \text{ s}^{-1}$. Note that negative values, which indicate reduction in density due to ice melt, are largely confined to a small region north of Denmark Strait. The ice distribution (Figure 2i) reveals a transition from relatively ice-free winter conditions in the western Barents Sea to 50–100% cover in the eastern Barents Sea.

Similar conclusions regarding the different components hold for the standard deviation of the mean field (determined for the set of all 1000 winters from the model control run). The thermal term tends to dominate variability in the western Barents, Greenland, and Norwegian Seas, with variability in the haline term being very small in comparison across the whole region. The ice melt term shows locally strong variability, in particular in the Denmark Strait and Greenland Sea regions close to the mean ice edge.

Properties of the water flowing through Fram Strait at 78.75°N in the model are shown in Figure 3. In the surface layer (0–500 m), two main currents are present. On the western side, cold Arctic surface waters flow southward in the East Greenland Current (EGC). Along the eastern margin, relatively warm Atlantic waters flow northward into the Arctic in the West Spitsbergen Current (WSC). The surface waters are relatively fresh and become more saline from west to east. This dominates the temperature effect on density, as there is an overall increase in surface layer density from west ($=25.0 \text{ kg m}^{-3}$) to east ($=27.9 \text{ kg m}^{-3}$) across the strait. The deeper waters (~ 500 – 2500 m) are dominated by southward flow with mean velocity up to 0.4 m s^{-1} at 1500 m .

Over the 1000 year period of the model simulation, the annual net oceanic full-depth volume transport is $0.8 \pm 0.5 \text{ Sv}$ to the south. This represents the difference between large northward ($10.5 \pm 1.6 \text{ Sv}$) and southward ($11.3 \pm 1.7 \text{ Sv}$) flows. These values are in reasonable agreement with observation-based estimates by Schauer *et al.* [2004] of 9–10 Sv northward and 12–13 Sv southward. The NAW inflow into the Barents Sea between Bear Island and Norway has also been compared with observations. The mean winter/summer volume transport is $1.8 \pm 1.1 \text{ Sv}/0.7 \pm 0.5 \text{ Sv}$ and agrees well with observations $1.7 \text{ Sv}/1.3 \text{ Sv}$ [Ingvaldsen *et al.*, 2004].

The control run winter mean flow at two levels (204 and 996 m) chosen to represent the intermediate and deep flow is shown in Figures 4a and 4b. The strong mean outflow from the Barents Sea to the Arctic through the St. Anna Trough is clearly evident at 204 m. The mean flow field at 996 m shows the southward transport through the Fram Strait. This will subsequently be shown to be enhanced in strong Barents Sea air-sea density flux winters. The HadCM3 bathymetry is also shown in both Figures 4a and 4b for reference. It may be compared with high-resolution observation-based bathymetry from the National Oceanic and Atmospheric Administration ETOPO2v2 data set (from <http://www.ngdc.noaa.gov/mgg/fliers/06magg01.html>) in Figure 4c. Although the model is relatively coarse, it can be seen to have a reasonable representation of the features evident in the observed fields given the difference in scales.

3.2. Extreme Surface Density Flux Events in the Barents Sea

A composite analysis has been carried out to investigate the characteristics of extreme winter Barents Sea surface density flux events and their potential impacts on the regional ocean circulation. A similar approach was taken in the studies of the Denmark Strait transport response to Greenland Sea surface heat loss noted in section 1 [Grist *et al.*, 2007, 2008]. We employ it again here for consistency with the earlier work. For this analysis, the density flux values are averaged over a Barents Sea box (27.5 – 51.25°E , 69.375 – 79.375°N , shown by the black solid box in Figure 2a).

For the full period of the HadCM3 control run, the time series of F_ρ averaged over the Barents Sea box is shown in Figure 5. The mean value for F_ρ is $3.8 \times 10^{-6} \text{ kg m}^{-2} \text{ s}^{-1}$ with a standard deviation of $6.5 \times 10^{-7} \text{ kg m}^{-2} \text{ s}^{-1}$. The 10 winters of strongest and weakest density flux were identified and are indicated by crosses in Figure 5. These winters are referred to as the SL and WL winters, respectively. This terminology was adopted in earlier work [Grist *et al.*, 2007, 2008] and reflects the strong and weak net air-sea heat losses that the winters exhibit (see below). For the SL winters, the mean $F_\rho = 5.4 \times 10^{-6} \text{ kg m}^{-2} \text{ s}^{-1}$ while for the WL subset, $F_\rho = 2.3 \times 10^{-6} \text{ kg m}^{-2} \text{ s}^{-1}$ (in each case the difference is greater than two standard deviations from the mean). The corresponding net heat flux value for the SL winters is $Q_{\text{net}} = -203 \text{ W m}^{-2}$ and for WL, $Q_{\text{net}} = -46 \text{ W m}^{-2}$. Thus, the winter mean net heat loss from the ocean to the atmosphere increases by 157 W m^{-2} between the two cases. This is primarily due to an increase in the combined latent and sensible heat loss by 107 W m^{-2} .

We note that the Barents Sea ice cover in HadCM3 tends to be greater than in the recent observational record. For example, the model winter mean ice cover for the Barents Sea box in SL years is 54.5%. In

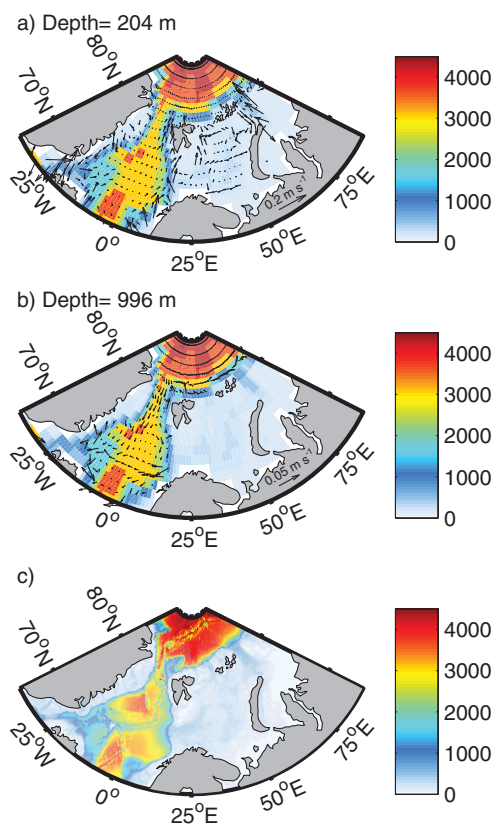


Figure 4. HADCM3 mean winter velocity (arrows) at: (a) 204 m, (b) 996 m. The model bathymetry (color field, units m) is overlaid in Figures 4a and 4b, with the bathymetry from the ETOPO2 data set displayed in Figure 4c.

has also been carried out using density flux fields from the NCEP/NCAR atmospheric reanalysis for the period 1950–2005, see Figures 6c and 6d. Note the definition of winter is such that 1950 refers to the combined months of December 1949 and January–March 1950; likewise for other winters. The reanalysis was not detrended. However, this does not lead to a problem with clustering at either end of the record as both the SL and WL subsets contain five winters prior to 1975, and five winters after 1975. Similar patterns to those found with HadCM3 are obtained using NCEP/NCAR for the SL and WL winters indicating that the model provides a reasonable qualitative representation of the surface density flux extremes. Note the difference in scales between the model and NCEP/NCAR panels. The latter are reduced in amplitude by about a factor 2 which may reflect the relatively short period (56 winters) used for the reanalysis composite when compared with the model (1000 winters). For further comparison, we have generated additional SL and WL composite plots from the model using winter subsets spanning the same length (56 winters) as the NCEP/NCAR reanalysis. It is possible to generate a total of 17 of these 56 winter subsets from the full 1000 year model run. The average over these subsets is shown in Figures 6e and 6f (now using the same color scale as Figures 6c and 6d). Reasonable qualitative and quantitative agreement with the NCEP/NCAR composites in Figures 6c and 6d may now be observed.

Changes in the ocean circulation at depth associated with the strong air-sea density flux years are examined in more detail by forming winter velocity anomaly maps on the 205 and 996 m model depth levels averaged over the SL subset, see Figure 7. In the SL years, there is an increase in both the northward intermediate depth flow out of the Barents Sea (Figure 7a) and the east-west deep flows north of Spitsbergen and south through the Fram Strait (Figure 7b). Note there is a change of scale by 30% between Figures 7a and 7b in order to improve the clarity of Figure 7b. The anomalous flow on the 996 m level is highlighted by showing all velocity anomaly vectors with magnitude greater than 0.005 m s^{-1} in red. This reveals an anomalous east to west flow north of Spitsbergen, originating in the SFJL Strait, which subsequently flows southward through Fram Strait toward the Norwegian Sea. In the WL composite (not shown), there is a weak

comparison, we have determined the winter mean ice cover from the HadISST observation-based data set [Rayner *et al.*, 2003] for 1980–2008 and find it to be 32.9%. However, the relatively high ice cover in the model does not prevent us from examining the impacts of the variations in winter air-sea heat exchange that are the main goal of our analysis. This is demonstrated by the large ranges in air-sea density and net heat flux between SL and WL years noted above.

Composite maps showing the anomaly of F_p from the 1000 year winter mean averaged over the SL and WL years are shown in Figures 6a and 6b. In the SL years, a coherent pattern of enhanced total density flux is evident in the Barents Sea region with individual grid cell F_p anomalies approaching $5 \times 10^{-6} \text{ kg m}^{-2} \text{ s}^{-1}$. A similar pattern with sign reversed is observed for the WL years, with negative anomalies as large as $-5 \times 10^{-6} \text{ kg m}^{-2} \text{ s}^{-1}$. The composite study

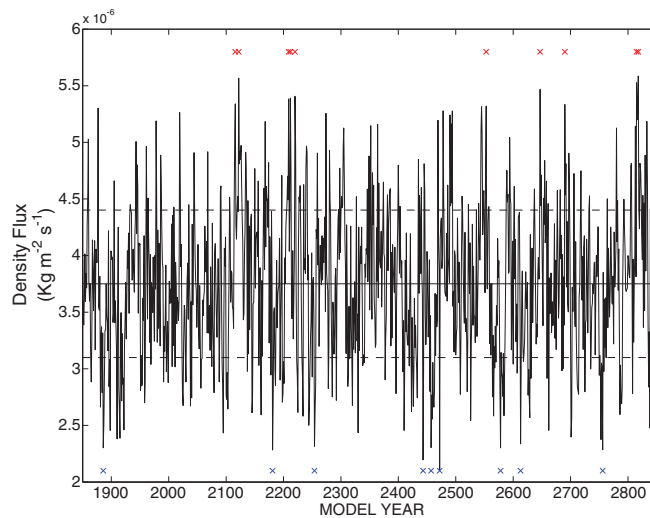


Figure 5. Time series of Barents Sea box winter (DJFM) mean total density flux, F_p , from the HadCM3 1000 year control run. Red/blue crosses denote the years of strongest/weakest density flux. The solid and dashed lines represent the mean density flux and ± 1 standard deviation from the mean.

anomalous flow at 996 m in the opposite, northward, direction toward Fram Strait. Note also that, in addition to the modified outflow, an anomalous cyclonic feature in the Barents Sea at the 205 m level is seen in Figure 7a. This indicates that the increased surface fluxes in SL years also modify the sub-basin scale circulation.

3.3. Barents Sea Surface Density Flux Impacts on Fram Strait Transport

The model results presented in Figure 7 suggest that extreme Barents Sea heat loss may increase the outflow through the SFJL Strait. Measurements in this region are lacking [Loeng *et al.*,

1997], so it is not possible to determine whether this response is supported by observations. However, the direction of the anomalous flow in the deeper layer in HadCM3 suggests that extreme Barents Sea heat loss may subsequently influence the transport through Fram Strait via a short time scale anomaly

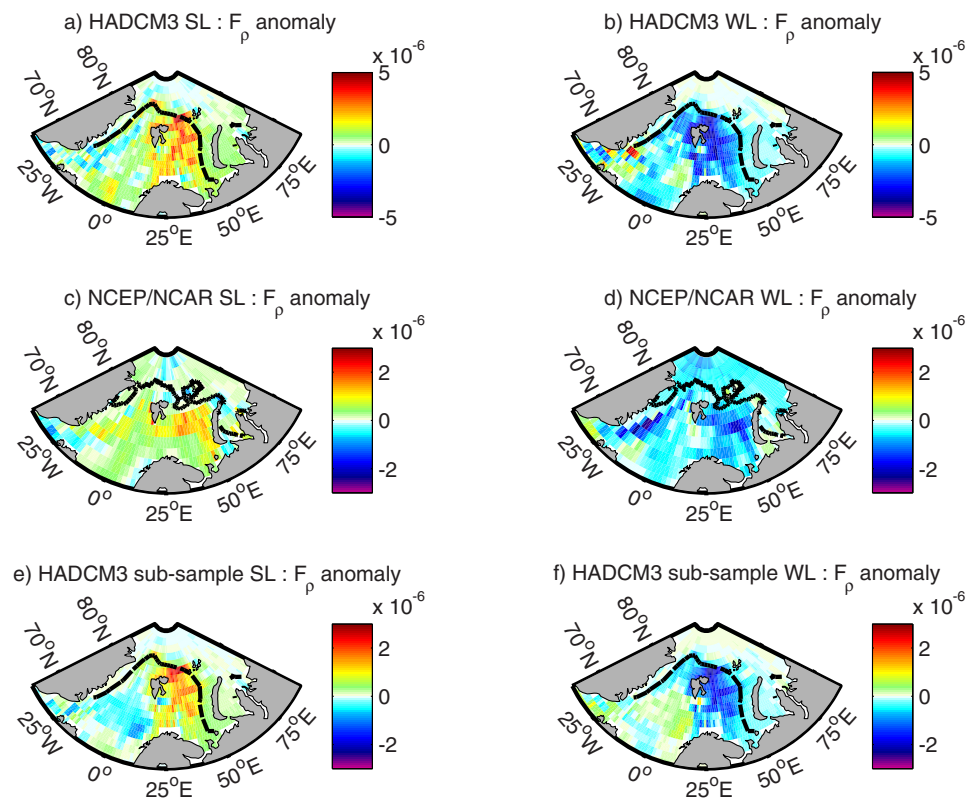


Figure 6. (a and b) Composite maps showing the anomaly of the HadCM3 total winter density flux from the 1000 year winter mean averaged over (a) the 10 strongest (SL) and (b) the 10 weakest (WL) surface density flux winters. Dashed lines as Figure 2 shows 95% ice extent. (c and d) Composite maps obtained from NCEP/NCAR reanalysis following the same approach but selecting the 10 SL and WL winters from the period 1950–2005. (e and f) As Figures 6a and 6b but now showing the average over 17 subsamples from HadCM3 each of which is of the same length (56 winters) as the NCEP/NCAR period considered.

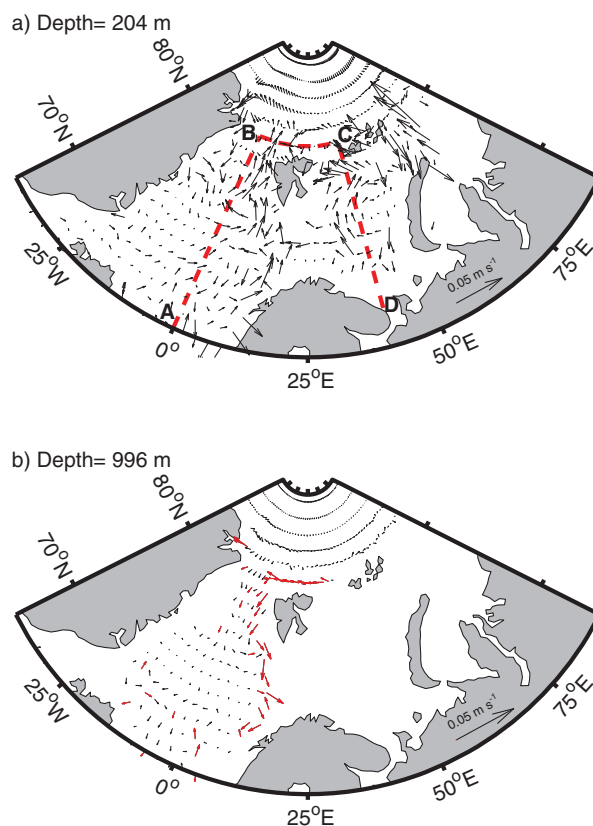


Figure 7. HADCM3 winter velocity anomalies at two depth levels averaged over the SL subset: (a) 204 m and (b) 996 m. The dashed line indicates the section displayed in Figure 11. The red vectors in Figure 7b indicate a velocity magnitude $>0.005 \text{ m s}^{-1}$ to highlight the anomalous southward flow.

propagated via the SFJL Strait. The composite circulation pattern is a winter velocity anomaly so a component of the anomalous flow occurs on a time scale of several months (i.e., within the winter in which the strong heat loss event occurs). However, the SL winters do not always occur in isolation as there is a tendency in some cases for them to occur with short interval gaps of several years (see Figure 5). Thus, the anomalous flow also reflects to some extent the combined contributions of closely separated winters and this makes it difficult to identify a characteristic time scale for the propagation from the composite analysis. This anomalous flow occurs in addition to the previously recognized longer time scale, of order 20 year anomaly, resulting from outflow through the St. Anna Trough that propagates around the Arctic Basin [Newton *et al.*, 2008; Smith *et al.*, 2011]. A detailed analysis of the relevant time scales requires further research using ocean model

runs perturbed with an anomalous Barents Sea density flux signal in a given winter to isolate the propagation of the circulation anomalies. We carried out such an analysis in our earlier study of processes affecting the Demark Strait overflow [Grist *et al.*, 2008] and plan to adopt a similar approach in subsequent work to fully determine the characteristic time scales for the Barents Sea influence on Fram Strait.

In the present study, we now employ a correlation analysis to examine whether variations in the transport through Fram Strait may be related to surface density flux variability in the adjacent ocean regions at short time scales. The correlation between annual mean southward winter volume transport through Fram Strait and surface density flux is shown in Figure 8. In order to focus on the deep southward flow, the low density, southward-flowing polar water (<27.0) on the Greenland shelf was removed before calculating the transport. The correlation coefficients shown are significant at the 99% level based on a (two-tailed) Student's *t* test. All the time series were detrended and autocorrelations were taken into account in determining the degrees of freedom for significance testing [Emery and Thomson, 1997].

The pattern for F_p shows a large region with positive correlations centered on the Barents Sea (Figure 8) with a maximum value $r = 0.40$. The pattern for F_T is broadly similar to that obtained for F_p as is to be expected given the strong contribution of F_T to the total density flux discussed earlier. The correlation values between F_T and the transport tend to be greater than those found with F_p . This indicates a stronger dependence of the Fram Strait transport on the thermal component of the density flux once the ice melt and haline terms are removed. In comparison, the correlation values between the transport and both F_S and F_{IM} are weaker than those found with F_T . The correlation pattern for F_S is somewhat similar to that for F_T . This is to be expected as F_S is dependent on evaporation and this also influences F_T via the latent heat flux (which is equivalent to the evaporation). The correlation pattern for F_{IM} is notably different to the others shown and exhibits a high degree of spatial variability with frequent changes in sign. Although the F_{IM} correlations for the Barents Sea are locally as high as in the other panels, they are of small spatial extent

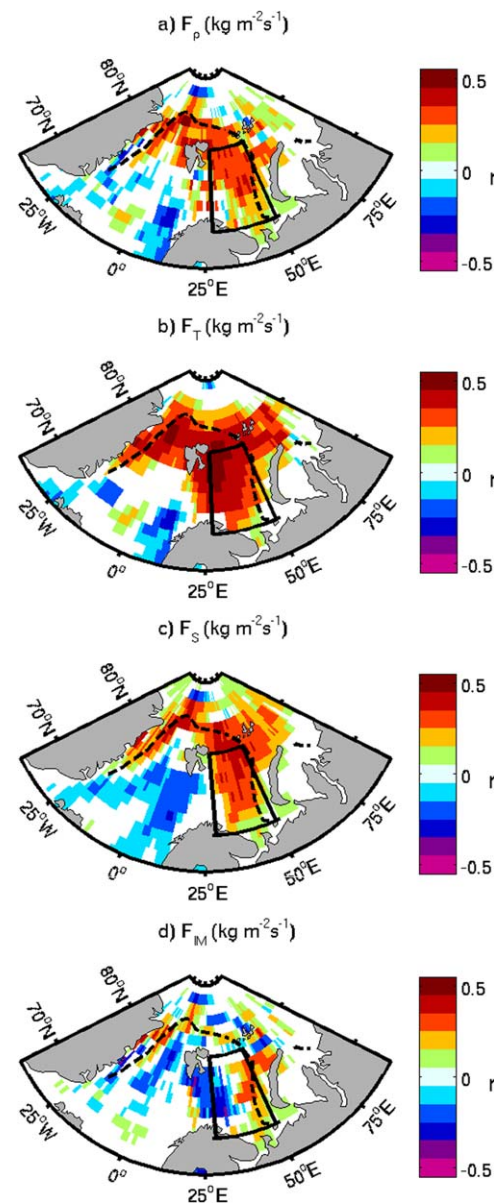


Figure 8. Correlation of the southward winter transport through the Fram Strait with: (a) F_ρ , (b) F_T , (c) F_S , and (d) F_M . Colored regions indicate correlation coefficient values that are significant at a 99% level. A positive (negative) value indicates an increase (decrease) in the mean Fram Strait southward transport coincident with an increase (decrease) in the surface density flux. Black solid and dashed lines as Figure 2.

play a major role in modifying the transport. The scatter plot for F_S is not shown as this term is much smaller in magnitude (maximum value $3 \times 10^{-7} \text{ kg m}^{-2} \text{ s}^{-1}$) than either of the other two terms and has a negligible contribution to the total winter density flux in the Barents Sea box.

We have investigated whether the Fram Strait temperature and salinity fields change at the time of strong Barents Sea air-sea density flux using composite anomaly fields for the SL subset in Figure 10. Coherent patterns of change are evident in the southward flowing water below 250 m which is colder by up to 0.5°C and fresher by up to 0.05 than the climatological winter mean. In addition, we show changes in temperature and along-track velocity in Figure 11 along a model section. The section runs from the Barents Sea northward through the SFJL Strait, then west to east along a line north of Spitsbergen and finally south through Fram Strait (section shown in Figure 7a). A coherent signal emerges with strong near surface out-flow (velocity anomalies up to 0.01 m/s) at 100–200 m depth in the north-south Barents Sea section (C–D).

suggesting that ice melt does not have as strong and coherent impact on the Fram Strait transport as F_T . This suggestion is supported by subsequent regression reported below (see discussion of Figure 8).

The Fram Strait winter southward transport anomaly has been calculated for each of the extreme density flux subsets introduced in section 3.2. For the SL years, there is an increase in the southward transport of 2.4 Sv and for the WL years there is a reduction of 1.0 Sv. More generally, the variation of the mean southward winter transport through Fram Strait with the Barents Sea box mean winter total density flux and its components is shown in Figure 9 for all years. An increase in transport with F_ρ is clearly seen ($r = 0.47$) and this is even more evident with F_T ($r = 0.52$). Such a relationship is to be expected if cooling of Barents Sea surface water via atmospheric heat loss results in production of dense water that subsequently leaves the region at depth toward the north-west and then propagates south through Fram Strait (as shown in Figure 6b). A linear fit to the relationship yields a Fram Strait southward transport increase of 1.22 Sv for an increase in F_T of $1 \times 10^{-6} \text{ kg m}^{-2} \text{ s}^{-1}$. For F_{IM} , the correlation with the southward volume transport is insignificant ($r = -0.07$). This indicates that variations in the ice melt buoyancy forcing do not

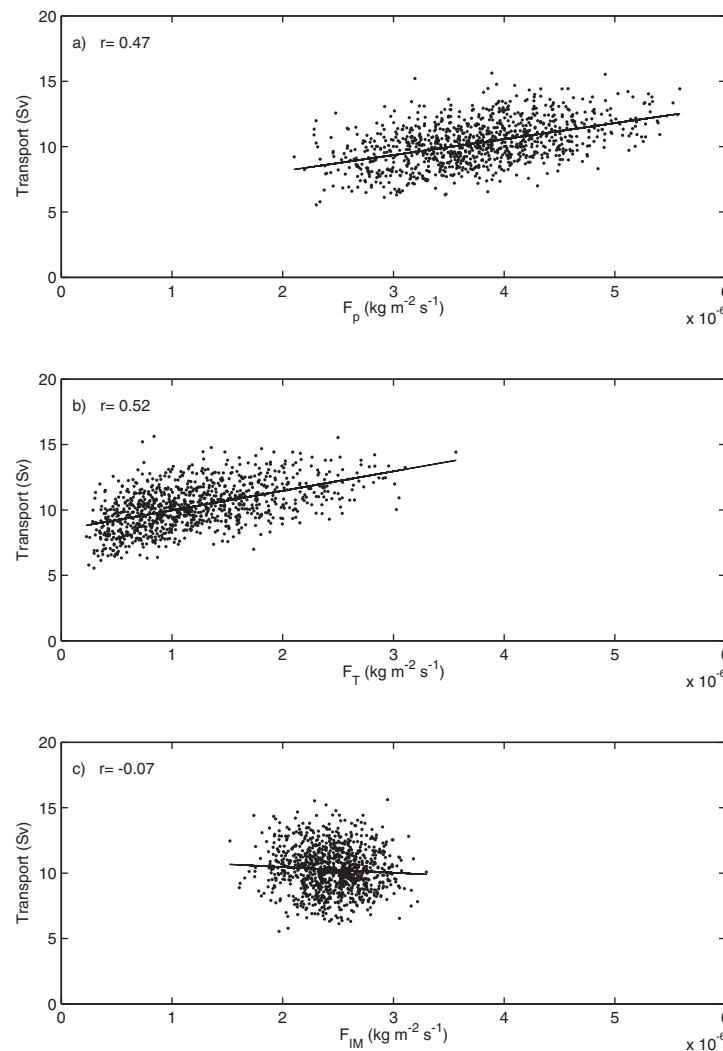


Figure 9. The variation of the mean southward winter transport through Fram Strait with the Barents Sea mean winter: (a) total density flux (F_p), (b) thermal component (F_T), and (c) ice melt component (F_{IM}). Linear regressions are fitted to the data and shown in each plot.

the north-westward intermediate depth flow out of the basin and the east-west deep flows north of Spitsbergen and south through the Fram Strait (Figure 7). For the 10 strongest Barents Sea surface density flux years, the Fram Strait winter southward transport increases by 2.4 Sv. This compares with a reduction of 1.0 Sv for the corresponding weak surface density flux years. Furthermore, the properties of the southward flowing water are modified under strong Barents Sea density flux conditions. The water below 250 m in the Fram Strait being colder by up to 0.5°C and fresher by 0.05 than the climatological winter mean.

Anomalies in the total surface density flux, F_p , in the Barents Sea arise primarily from the thermal term, F_T . The other two terms (haline and ice formation) play a relatively minor role. The strength of this relationship has been quantified by considering air-sea density flux values averaged over a Barents Sea regional box. The value of the correlation coefficient between the Fram Strait dense southward flow and the box averaged F_T is $r = 0.52$. Thus, about 25% of the variance in the flow may be explained via variability in the winter air-sea density flux forcing of the Barents Sea.

The results that we have obtained show the response of the Barents Sea circulation to extreme air-sea exchanges in a long (millennial timescale) control run of a coupled ocean-atmosphere model. The modified outflow through the Spitsbergen-Franz Josef Land Strait following extreme Barents Sea heat loss and its subsequent impact on the Fram Strait transport has not previously been recognized. Given the long nature

These persist at deeper levels, peaking at 1000 m in the east-west section north of Spitsbergen (B–C) and are accompanied by cold temperatures of 0.2–0.3°C. Cold anomalies are also evident in the deep layers (1500–3000 m) south of Fram Strait (A–B) although the velocity signal is less clear here which may reflect the effects of mixing.

4. Summary

The aim of this study has primarily been to examine how the Barents Sea circulation responds to a wide range of air-sea density flux forcing as realized by a 1000 year control run of the HadCM3 coupled ocean-atmosphere model. The long control run has enabled a wide range of air-sea interaction conditions to be sampled and the intention has not been to directly represent conditions in the recent decades of strong sea-ice loss in the Barents Sea.

We have analyzed the difference in ocean circulation between years with extreme strong and weak Barents Sea surface density flux. This reveals an increase in both

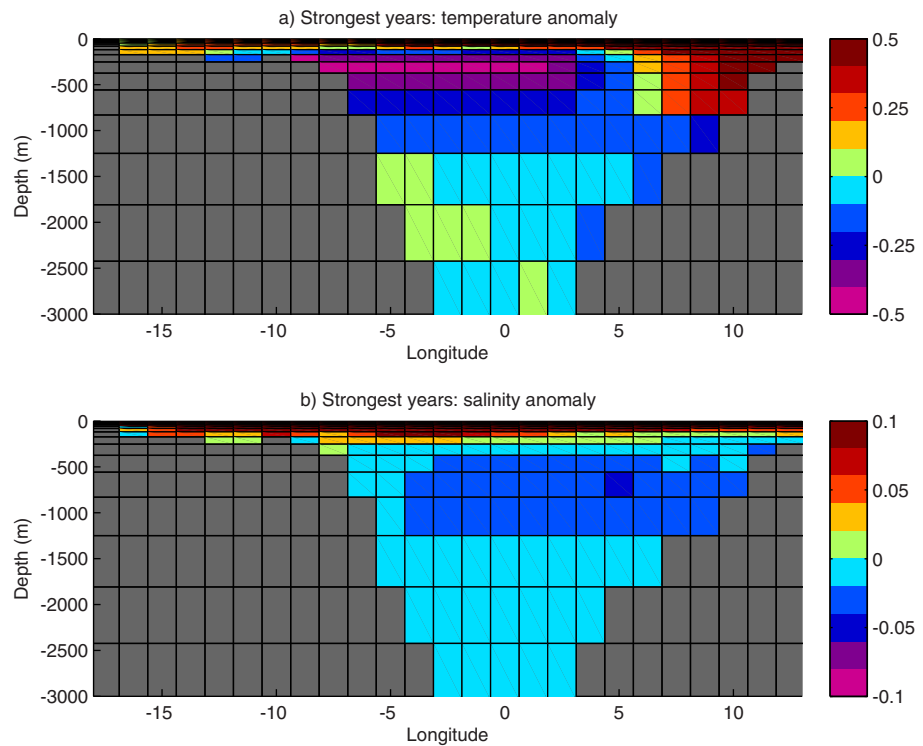


Figure 10. Fram Strait section composite fields showing the anomalies from the 1000 year winter mean of (a) temperature and (b) salinity averaged over the SL winter subset.

of the run we are not, at present, able to say whether the results are of direct relevance to changes in the Barents Sea region in recent decades. In future work, we aim to make this connection by examining whether a similar Barents Sea outflow modification occurs in a high-resolution ocean model (1/12° NEMO, *Deshayes et al.* [2013]) forced by observed surface flux fields since the late 1980s.

Our analysis indicates that surface density flux variations in the Barents Sea, primarily driven by changes in the net air-sea heat flux, are potentially important for the regional circulation. In the coupled model run

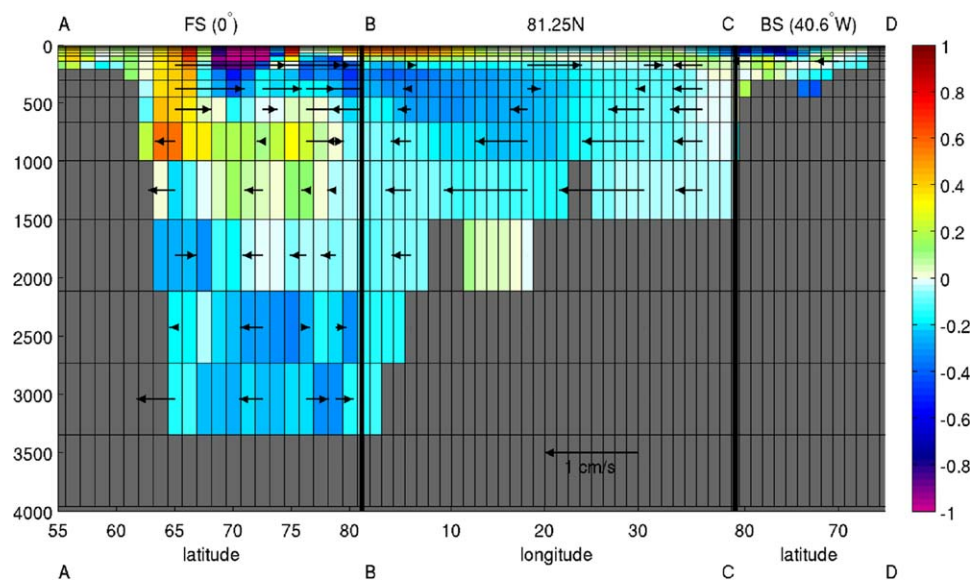


Figure 11. Anomalous temperature and along-track velocity anomaly for the SL year subset along a model section running from the Barents Sea northward through the SFJL Strait (D to C), along an east-west line north of Spitsbergen (C to B) and then south through Fram Strait (B to A). Note: the section is shown in Figure 7a.

considered here, they have an impact on the southward transport through Fram Strait on a time scale of order a year. Assessing whether this mechanism operates in the real world given changes in ice cover in the Barents Sea in recent decades is an interesting question for ongoing research.

Acknowledgment

This research was funded by the UK Natural Environment Research Council.

References

- Aksenov, Y., V. V. Ivanov, A. J. Nurser, S. Bacon, I. V. Polyakov, A. C. Coward, A. C. Naveira-Garabato, and A. Beszczynska-Moeller (2011), The Arctic circumpolar boundary current, *J. Geophys. Res.*, *116*, C09017, doi:10.1029/2011JC006637.
- Årthun, M., T. Eldevik, L. Smedsrud, Ø. Skagseth, and R. Ingvaldsen (2012), Quantifying the influence of Atlantic heat on Barents Sea ice variability and retreat, *J. Clim.*, *25*, 4736–4743, doi:10.1175/JCLI-D-11-00466.1.
- Beszczynska-Möller, A., E. Fahrbach, U. Schauer, and E. Hansen (2012), Variability in Atlantic water temperature and transport at the entrance to the Arctic Ocean, 1997–2010, *ICES J. Mar. Sci.*, *69*, 852–863.
- Cavalieri, D. J., and C. L. Parkinson (2012), Arctic sea ice variability and trends, 1979–2010, *Cryosphere*, *6*, 881–889, doi:10.5194/tc-6-881-2012.
- Day, J. J., J. L. Bamber, P. J. Valdes, and J. Kohler (2012), The impact of a seasonally ice free Arctic Ocean on the temperature, precipitation and surface mass balance of Svalbard, *Cryosphere*, *6*, 35–50, doi:10.5194/tc-6-35-2012.
- Deshayes, J., et al. (2013), Oceanic hindcast simulations at high resolution suggest that the Atlantic MOC is bistable, *Geophys. Res. Lett.*, *40*, 3069–3073, doi:10.1002/grl.50534.
- Emery W. J., and R. E. Thomson (1997), *Data Analysis Methods in Physical Oceanography*, 634 pp., Pergamon, Oxford, U. K.
- Giles, K. A., S. W. Laxon, A. L. Ridout, D. J. Wingham, and S. Bacon (2012), Western Arctic Ocean freshwater storage increased by wind-driven spin-up of the Beaufort Gyre, *Nat. Geosci.*, *5*, 194–197, doi:10.1038/ngeo1379.
- Gill, A. E. (1982), *Atmosphere-Ocean Dynamics*, Int. Geophys. Ser., vol. 30, 662 pp., Elsevier, New York.
- Gordon, C., C. Cooper, C. A. Senior, H. Banks, J. M. Gregory, T. C. Johns, J. F. B. Mitchell, and R. A. Wood (2000), The simulation of SST, sea ice extents and ocean heat transports in a version of the Hadley Centre coupled model without flux adjustments, *Clim. Dyn.*, *16*, 147–168, doi:10.1007/s003820050010.
- Gregory, J. M., P. A. Stott, D. J. Cresswell, N. A. Rayner, C. Gordon, and D. M. H. Sexton (2002), Recent and future changes in Arctic sea ice simulated by the HadCM3 AOGCM, *Geophys. Res. Lett.*, *29*(24), 2175, doi:10.1029/2001GRL014575.
- Grist, J. P., S. A. Josey, and B. Sinha (2007), Impact of the ocean of extreme Greenland Sea Heat loss in the HadCM3 coupled ocean-atmosphere model, *J. Geophys. Res.*, *112*, C04014, doi:10.1029/2006JC003629.
- Grist, J. P., S. A. Josey, B. Sinha, and A. T. Blaker (2008), Response of the Denmark Strait overflow to Nordic Seas heat loss, *J. Geophys. Res.*, *113*, C09019, doi:10.1029/2007JC004625.
- Holliday, N. P., et al. (2008), Reversal of the 1960s to 1990s freshening trend in the northeast North Atlantic and Nordic Seas, *Geophys. Res. Lett.*, *35*, L03614, doi:10.1029/2007GL032675.
- Ingvaldsen, R. B., L. Asplin, and H. Loeng (2004), The seasonal cycle in the Atlantic transport to the Barents Sea during the years 1997–2001, *Cont. Shelf Res.*, *24*, 1015–1032, doi:10.1016/j.csr.2004.02.011.
- Loeng, H., V. Ozhigin, and B. Ådlandsvik (1997), Water fluxes through the Barents Sea, *ICES J. Mar. Sci.*, *54*, 310–317.
- Myers, P. G. (2005), Impact of freshwater from the Canadian Arctic archipelago on Labrador Sea water formation, *Geophys. Res. Lett.*, *32*, L06605, doi:10.1029/2004GL02282.
- Newton, R., P. Schlosser, D. G. Martinson, and W. Maslowski (2008), Freshwater distribution in the Arctic Ocean: Simulation with a high resolution model and model-data comparison, *J. Geophys. Res.*, *113*, C05024, doi:10.1029/2007JC004111.
- Rayner, N., D. Parker, E. Horton, C. Folland, L. Alexander, D. Rowell, E. Kent, and A. Kaplan (2003) Global analyses of SST, sea ice, and night marine air temperature since the late 19th century, *J. Geophys. Res.*, *108*(D14), 4407, doi:10.1029/2002JD002670.
- Ridley, J. K., J. A. Lowe, and H. T. Hewitt, (2012), How reversible is sea ice loss, *Cryosphere*, *6*, 193–198.
- Rudels, B., P. E. Jones, U. Schauer, and P. Eriksson (2004), Atlantic sources of the Arctic Ocean surface and halocline waters, *Polar Res.*, *23*, 181–208.
- Schauer, U., R. D. Muench, B. Rudels, and L. Timokhov (1997), Impact of Eastern Arctic shelf waters on the Nansen Basin intermediate layers, *J. Geophys. Res.*, *102*, 3371–3382, doi:10.1029/96JC03366.
- Schauer, U., H. Loeng, B. Rudels, V. K. Ozhigin, and W. Dieck (2002), Atlantic Water flow through the Barents and Kara Seas, *Deep Sea Res., Part I*, *49*, 2281–2298.
- Schauer, U., E. Fahrbach, S. Osterhus, and G. Rohardt (2004), Arctic warming through the Fram Strait: Oceanic heat transport from 3 years of measurements, *J. Geophys. Res.*, *109*, C06026, doi:10.1029/2003JC001823.
- Sinha, B., B. Toplis, A. T. Blaker, and J.-M. Hirschi (2013), A numerical model study of the effects of interannual time scale wave propagation on the predictability of the Atlantic meridional overturning circulation, *J. Geophys. Res.*, *118*, 131–146, doi:10.1029/2012JC008334.
- Smedsrud, L. H., R. Ingvaldsen, J. E. O. Nilsen, and O. Skagseth (2010), Heat in the Barents Sea: Transport, storage, and surface fluxes, *Ocean Sci.*, *6*, 219–234.
- Smith J. N., F. A. McLaughlin, W. M. Smethie Jr., S. B. Moran, and K. Lepore (2011), Iodine-129, ¹³⁷Cs, and CFC-11 tracer transit time distributions in the Arctic Ocean, *J. Geophys. Res.*, *116*, C04024, doi:10.1029/2010JC006471.
- Stouffer, R. J., et al. (2006), Investigating the causes of the response of the thermohaline circulation to past and future climate changes, *J. Clim.*, *19*(8), 1365–1387.
- Stroeve, J. C., V. Kattsov, A. Barrett, M. Serreze, T. Pavlova, M. Holland, and W. N. Meier (2012), Trends in Arctic sea ice extent from CMIP5, CMIP3 and observations, *Geophys. Res. Lett.*, *39*, L16502, doi:10.1029/2012GL052676.
- Vellinga, M., and R. A. Wood (2002), Global Climatic impacts of a collapse of the Atlantic thermohaline circulation, *Clim. Change*, *54*, 251–267.
- Walcowski, W., and J. Piechura (2007), Pathways of the Greenland Sea warming, *Geophys. Res. Lett.*, *34*, L10608, doi:10.1029/2007GL029974.
- Wang, M., and J. E. Overland (2009), A sea ice free summer Arctic within 30 years?, *Geophys. Res. Lett.*, *36*, L07502, doi:10.1029/2009GL037820.
- Wu, P., R. Wood, and P. Stott (2005), Human influence on increasing Arctic river discharges, *Geophys. Res. Lett.*, *32*, L02703, doi:10.1029/2004GRL021570.